Vertical shears in Saturn's eastward jets at cloud level

Enrique García-Melendo, Agustín Sánchez-Lavega, J.F. Rojas, S. Pérez-Hoyos, R. Hueso

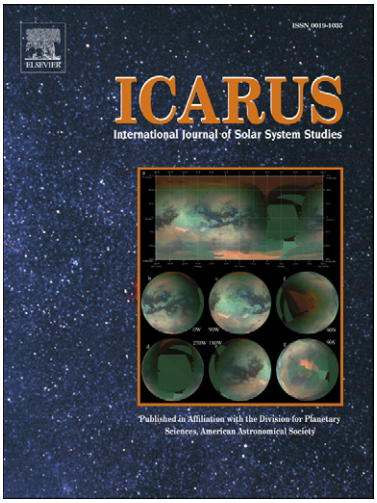

Vertical shears in Saturn's eastward jets at cloud level

Enrique García-Melendo, Agustín Sánchez–Lavega, J.F. Rojas, S. Pérez-Hoyos, R. Hueso

PII: S0019-1035(09)00084-0
DOI: 10.1016/j.icarus.2009.02.022
Reference: YICAR 8937

To appear in: *Icarus*

Received date: 10 September 2008
Revised date: 27 February 2009
Accepted date: 27 February 2009

Please cite this article as: E. García-Melendo, A. Sánchez–Lavega, J.F. Rojas, S. Pérez-Hoyos, R. Hueso, Vertical shears in Saturn's eastward jets at cloud level, *Icarus* (2009), doi: 10.1016/j.icarus.2009.02.022

VERTICAL SHEARS IN SATURN'S EASTWARD JETS AT CLOUD LEVEL

Enrique García-Melendo
Esteve Duran Observatory Foundation
08553 Seva, Spain

Agustín Sánchez–Lavega
Departamento de Física Aplicada I, E.T.S. Ingenieros, Universidad del País Vasco, Alameda Urquijo s/n, 48013 Bilbao, Spain

J. F. Rojas
Departamento de. Física Aplicada I, E.U.I.T.I., Universidad País Vasco, Bilbao Spain

S. Pérez-Hoyos
Departamento de Física Aplicada I, E.T.S. Ingenieros, Universidad del País Vasco, Alameda Urquijo s/n, 48013 Bilbao, Spain

R. Hueso
Departamento de Física Aplicada I, E.T.S. Ingenieros, Universidad del País Vasco, Alameda Urquijo s/n, 48013 Bilbao, Spain

Submitted to *Icarus*

Submitted: 10 September 2008

Revised: 26 february 2009

Proposed Running Head: Saturn's Atmosphere wind shear

Editorial correspondence to:

Dr. Enrique García-Melendo

Esteve Duran Observatory Foundation

Montseny 46

08533 Seva

Spain

E-mail: egarcia@foed.org

Abstract

We have measured the vertical shear of the zonal winds in the cloud-haze upper layer of Saturn using Cassini ISS images obtained in the filters MT2 (753 nm methane absorption band, sensitive to the upper haze) and CB2 (adjacent continuum, sensitive to the lower cloud). Our radiative transfer models indicate that at the eastward jet peaks these filters are sensing clouds at the respective ~100 mbar and ~350 mbar levels. We have found a systematic velocity difference between those filters of 15 to 20 ms^{-1} only in the eastward jets peaks (27ºS, 42ºS, 55ºS and 70ºS) which implies a vertical shear of ~10-20 $ms^{-1}H^{-1}$. Our overall results agree with those derived from the thermal-wind relationship using CIRS thermal data (Fletcher et al. 2008) and with previous equatorial measurements (Sanchez-Lavega et al. 2007).

1. Introduction

The vertical structure of the zonal wind systems in Jupiter and Saturn and their relationship with the latitudinally alternating band pattern of the upper clouds and haze layers (belts and zones) is still a major open issue. In both planets the zonal winds above the clouds decrease with altitude over the range accessible to remote sensing (from ~1 mbar to ~1 bar). This was initially derived from measurements of the meridional temperature structure at different levels and the application of the thermal wind equation for geostrophic conditions (e.g. for Saturn, Conrath and Pirraglia, 1983). This technique has some limitations: first, it is not applicable close to the equator where geostrophy drops (it must be applied to latitudes above about ± 10º) and second, although wind shear is directly detectable from the temperature field, retrieving absolute

wind values requires a reference wind usually measured from cloud tracking motions at a unique reference altitude which is not precisely determined (for Saturn it can be somewhere in the pressure range ~ 0.2 to 1 bar), that in addition changes with latitude and time.

Measurement of atmospheric motions at different levels by cloud tracking in Jupiter and Saturn is not an easy issue since individual features within the optically thick cloud deck are mostly concentrated in a scale height (20-40 km), and in general, the shears between these thickness limits are not strong enough to precisely separate velocity differences. Nevertheless, Saturn is a better case; the clouds and hazes may extend vertically from two to three scale heights (~ 100 km, Sanchez-Lavega et al., 2004a; Pérez-Hoyos et al., 2005). This gives the chance to have in Saturn compact clouds at vertically separated locations, therefore moving as tracers of the wind speeds at their respective vertical position. Most features tracked in Saturn's atmosphere are supposed to be placed in the cloud deck (Ingersoll et al., 1984) putatively formed by ammonia ice or in the extended haze of the upper troposphere (Sánchez-Lavega et al., 2004b; Pérez-Hoyos and Sánchez-Lavega, 2006; Sánchez-Lavega et al., 2007). Tracers are mainly detected in the continuum green-red wavelength range (500–950 nm). Cloud tracking of deeper features (located in the pressure altitude range ~ 2–4 bars) can only be performed in the 5-μm spectral window (Yanamandra-Fisher et al., 2001; Baines et al., 2007) but full hemispheric coverage is not available yet to establish a wind shear structure. Above the ammonia cloud, higher hazes are detected in the UV range (250–350 nm) above the 100 mbar level and in the methane absorption bands (725 and 890 nm, and 2.3 μm) which sound levels close to the tropopause (60-150 mbar) and much higher (about 20-30 mbar) in the latter case. Individual features have been observed and tracked in the equatorial upper haze at 50 mbar in Hubble Space Telescope (Sánchez-

Lavega et al., 2003 and 2004b) and Cassini images (Porco et al., 2005; Sánchez-Lavega et al., 2007), finding a vertical shear for the zonal wind in the equatorial band (latitude range 5ºN – 10ºS) of ~ 40 ms^{-1} per scale height (H ~ 40 km). Voyager observation levels in the visible are more difficult to constrain because of the lack of images obtained with the appropriate filters sensitive to cloud and haze altitudes (Pérez-Hoyos et al., 2006).

2. Observations and wind measurements

We used Cassini images obtained in two filters sensing two altitude ranges: the methane absorption band filter MT2 (727 nm) sensitive to the upper tropospheric haze, and the continuum wavelength CB2 (752 nm) sensitive to lower levels, probably the lower tropospheric haze and upper cloud level (see section 3). Observations correspond to Cassini Orbiter ISS volumes 2006 and 2012 (from 2004-09-06 to 2004-09-19 and from 2005-06-15 to 2005-06-16 respectively) and show either full disk viewing with complete southern hemisphere coverage (COISS 2012) or a partial view at higher resolution of the southern hemisphere (COISS 2006). In both cases the selected images contain either a complete limb or a broad limb arc used for image navigation. For analysis of the images (limb location, disk orientation and longitude and latitude retrieval) we used the software PLIA (Hueso et al., *submitted*) assuming an oblate spheroid with respective equatorial and polar radii of 60268.0 km and 54364.0 km at the 1 bar pressure level (Lindal et al. 1985). The images were then projected in cylindrical and polar maps with resolutions similar to that of the original images, typically ~0.1deg·pix^{-1} and ~0.05degpix^{-1} in some cases.

To measure winds, we used a correlation technique in which East-West reflectivity scans obtained in 0.1º latitude steps are compared with similar scans at the

same latitude taken approximately one planetary rotation later (~10 hr). The position of the cross-correlation maximum between scan pairs constitutes an average measurement of the zonal motion of all cloud features in the scans, which can then be transformed into wind speeds relative to the Voyager rotation frame System III, and plotted in a meridional zonal wind profile for both filters (Figure 1). The method is fully described in García-Melendo and Sánchez-Lavega (2001). To get a good statistical result we used between 15 and 25 pairs of images averaging the results to get the mean wind velocity at each latitude and its r.m.s. This places our error bar for wind determination in ±5.0 ms^{-1}. Latitude errors in the profile arising from navigation of the images are lower than ±0.1º.

Our wind measurements in both filters cover the latitude range from 0º to 80ºS. It is evident from Figure 1 that the CB2 and MT2 wind profiles differ essentially in the peaks of the Eastward jets. To make this clearer we have plotted the wind difference between the two profiles as shown in Figure 1b. First, we retrieve and confirm the 100 ms^{-1} wind velocity difference in the equatorial jet (higher speeds in CB2) found in previous studies that used individual cloud tracking as a method for wind determination (Porco et al., 2005; Pérez-Hoyos et al., 2006; Sánchez-Lavega et al., 2007). Second, we see that at all the peaks of the eastward jets at the planetocentric latitudes 27ºS, 42ºS, 55ºS and 70ºS (excluding the equatorial jet), show significant deviations from the zero value that correspond on the average to speed differences of about 20 ms^{-1} higher in CB2 profiles than in MT2 profiles. There are other latitudes where deviations are of the order of 10 ms^{-1}, i.e. above the quoted errors in wind speed and latitudes, but we do not see a systematic relation with the westward jets or with the jet edges and they are probably spurious. We also visually identified and tracked individual tracers in image pairs examining the jet peaks and the intermediate regions. Individual measurements

fall on the measured correlation profiles. The bottom panel in Figure 1 illustrates different details observed in the MT2 and CB2 filters that move at different speeds at the jet peaks. Outside the jet peaks details observed in both MT2 and CB2 filters or observed only in MT2 or in CB2 move at the same speed.

[Figure 1]

3. Reflectivity scans and altitude level in the eastward jets

In order to study the altitude levels sampled in each filter at different latitudes we selected images corresponding to June 15, 2005 with a global view of the Southern hemisphere. The images were photometrically calibrated using the software CISSCAL V.3.3 (see Porco et al., 2004) and cylindrically projected with PLIA to extract absolute reflectivity scans (*I/F*) in the zonal and meridional directions in both filters. In the MT2 meridional scan the belt/zone pattern is evident, with a prominently bright Equatorial Zone. This pattern is practically indistinguishable in CB2 where the reflectivity profile is nearly flat. This difference is an evidence for separating the aerosol population into two distinct families: a haze at the upper levels and a cloud at the bottom. Except for the equatorial jet, the peak of the other jets divides the band where it resides in two regions, one bright equatorward of the jet peak and other dark poleward of the peak (Figure 1c).

We used a radiative transfer model and previous long-term results for Saturn's cloud and haze vertical structure (Acarreta and Sánchez-Lavega, 1999; Pérez-Hoyos et al., 2005; Karkoschka and Tomasko 2005) to retrieve the altitude and optical depth differences at both sides of the jet peak. The model considers a deep semi-infinite ammonia cloud with base at 1.4 bar made up by isotropic particles and above it, an extended tropospheric haze described by a double Henyey-Greenstein phase function

Our model atmosphere has only two adjustable parameters: the top pressure level of the tropospheric haze (from 60 mbar to 200 mbar in 20 mbar steps) and its total optical thickness (from 0 to 20 in 0.5 steps). We scanned the free parameter space and computed the r.m.s. deviation between model and observations with a 1% tolerance in the error. The combination of the continuum (sensitive to the optical thickness) and the methane absorption (sensitive to the top pressure value) allows a good constraint of this simple model atmosphere. This was done for the four jets and their neighbouring regions. An example of the procedure is shown in Figure 2.

[Figure 2]

With the obtained values we computed the total optical depth (including Rayleigh scattering, methane absorption and particle absorption and scattering) as a function of pressure for the atmosphere (on average: $P_{top} \sim 100$ mbar, $\tau \sim 5$) and found that the pressure levels with optical depth equal to unity is about 250 mbar for the MT2 observations and about 350 mbar for CB2 observations (height difference ~ 0.3 H) with little or none latitudinal dependence. This represents a good estimation for features with similar morphology in MT2 and CB2 images. However, features observed in MT2 that are not visible in CB2 (Figure 1) are probably caused by height variations in the upper levels of the tropospheric haze, as previously reported for equatorial features (Sánchez-Lavega et al., 2004). Features that are only observed in CB2 images should be deeper than the level where the atmosphere becomes optically thick ($\tau = 1$, at about 350 mbar), closer to the ammonia cloud. We provide in Table 1 realistic estimations of the levels sensed with each filter at the jet latitudes resulting in an average separation of 1.3 H between both levels when visible features in MT2 are placed on the top of the tropospheric haze. An in-depth analysis using all Cassini instrumentation able to

determine the vertical cloud structure could provide in a near future a better constraint on the sensing levels and therefore merits further research.

[Table 1]

4. Vertical shear and comparison with the thermal-wind results

These results extend to the southern jets up to the explored 80ºS latitude the effect found at the equatorial jet but at a reduced scale. Given the different pressure levels sensed by the MT2 and CB2 filters, it seems to be direct evidence for the vertical shear of the zonal winds, directly related to the thermal wind effect. Conrath and Pirraglia (1983) used the thermal-wind relationship to show that in Saturn's mid-latitude jets the zonal wind might decrease with altitude above the 150-500 mbar level at a rate $\partial u/\partial z = 10$ ms^{-1}/H. This has been recently estimated again by Flasar et al. (2005) and Fletcher et al. (2008) using Cassini CIRS data who computed vertical wind shears ~ 5 ms^{-1}/H. Our analysis shows a possible wind decay and indicates that the mid-latitude eastward jets (in the southern hemisphere) show this effect with $\partial u/\partial z$ = 10-20 ms^{-1}/H. This shear is lower than what we found in the equatorial jet where $\partial u/\partial z \sim 40$ms^{-1}/H (or 100 ms^{-1} wind speed difference between 700 and 50 mbar), but higher than the Cassini CIRS results. Wind measurements, performed with a 0.1º precision show that possible wind shear is confined within ~3º bands centered around the mid-latitude jet peaks. Due to the resolution difference between our direct wind measurements and the Cassini temperature data used in thermal wind computations these results do not need to be necessarily incompatible. By smoothing our correlation-derived wind profiles using a 2º window similar to the resolution of CIRS data, velocity differences at the jet peaks out of the equatorial region smooth down to ~ 5 to 7 ms^{-1}. Although thermal wind decay seems to be the main reason explaining the differences between both wind profiles,

there can be other mechanisms at play such as wave motions which might superimpose to the background zonal winds, and favor cloud formation at different pressure levels at the jet peaks (Sánchez-Lavega et al., 2006). However, these waves have not yet been identified.

From a photometric point of view, our analysis indicates that the eastward jet peaks divide the latitude band in two contrasted albedo bands in MT2 (methane absorption band at 725 nm): bright equatorwards side (slightly higher or abundant aerosol, ascending motions on the anticyclonic side) and dark polewards side (lower altitude or few aerosol, descending motions on the cyclonic side). These results are fully consistent with the simple model proposed by Conrath and Pirraglia (1983) of jets decaying with altitude and related vertical and meridional circulations. It is also consistent with the analysis of the temperature field in Fletcher et al. (2007) and it also throws a correlation between albedo and zonal winds similar to that found in Jupiter which probably merits further research.

Acknowledgements

This work has been funded by Spanish MEC AYA2006-07735 with FEDER support and Grupos Gobierno Vasco IT-464-07. RH acknowledges a “Ramón y Cajal” contract from MEC.

References

Acarreta, J.R. and A. Sánchez-Lavega 1999. Vertical cloud structure in Saturn's 1990 equatorial storm. *Icarus* **137**, 24 – 33.

Baines K., T. Momary, M. Roos-Serote, S. Atreya, R. Brown, B. Buratti, R. Clark P. Nicholson, 2007. Saturn's Polar Hexagon at depth: New images of stationary planetary waves in the North Polar Region by Cassini/VIMS *Geophys. Res. Abstr.* **9**, 02109.

Conrath, B.J., Pirraglia, J.A., 1983. Thermal structure of Saturn from Voyager infrared measurements—Implications for atmospheric dynamics. Icarus **53**, 286–292.

Flasar, F.M., and 45 colleagues, 2005. Temperatures, winds, and composition in the saturnian system. *Science* **307**, 1247–1251.

Fletcher, L.N., P.G.J. Irwin, N.A. Teanby, G.S. Orton, P.D. Parrish, R. de Kok, C. Howett, S.B. Calcutt, N. Bowles and F.W. Taylor, 2007. Characterising Saturn's vertical temperature structure from Cassini/CIRS *Icarus* **189**, 457 – 478.

Fletcher, L.N. and 13 colleagues, 2008. Temperature and composition of Saturn's polar hot spots and hexagon. *Science* **319**, 79 – 81.

García-Melendo, E. and A. Sánchez-Lavega 2001. A study of the stability of the Jovian zonal winds from HST images:1995-2000. *Icarus* **152**, 316 – 330.

Ingersoll, A.P., Beebe, R.F., Conrath, B.J., Hunt, G.E., 1984. Structure and dynamics of Saturn's atmosphere. In: Gehrels, T., Matthews, M.S. (Eds.), Saturn. Univ. of Arizona Press, Tucson, pp. 195–238.

Karkoschka, E. and M.G. Tomasko 2005. Saturn's vertical and latitudinal cloud structure 1991 – 2004 from HST imaging in 30 filters. *Icarus* **179**, 195 – 221.

Lindal, G. F., D. N. Sweetnam, and V. R. Eshleman 1985. The atmosphere of Saturn: An analysis of the Voyager radio occultation measurements. *Astron. J.* **90**, 1136–1146.

Pérez-Hoyos, S., A. Sánchez-Lavega, J.F. Rojas and R.G. French 2005. Saturn's cloud structure and temporal evolution from ten years of Hubble Space Telescope observations (1994 – 2003). *Icarus* **176**, 155 – 174.

Pérez-Hoyos, S. and A. Sánchez-Lavega 2006. On the vertical wind shear of Saturn's equatorial jet at cloud level. *Icarus* **180**, 161 – 175.

Porco, C. C. and 20 colleagues, 2004. Cassini imaging science: instrument characteristics and anticipated scientific investigations at Saturn. *Space Science Reviews* **115**, 363 – 497.

Porco, C., and 34 colleagues, 2005. Cassini imaging science: Initial results on

Saturn's atmosphere. *Science* **307**, 1243–1247.

Sánchez-Lavega, A., S. Pérez-Hoyos, J.F. Rojas, R. Hueso and R.G. French 2003. A strong decrease in Saturn's equatorial jet at cloud level. *Nature* **423**, 623 – 625.

Sánchez-Lavega A., S. Pérez-Hoyos, R. Hueso 2004a. Condensate clouds in planetary atmospheres: a useful application of the Clausius-Clapeyron equation, *Am. J. Phys.,* **72**, 767-774.

Sánchez-Lavega, A., R. Hueso, S. Pérez-Hoyos, J.F. Rojas and R.G. French 2004b. Saturn's cloud morphology before the Cassini encounter. *Icarus* **170**, 519 – 523.

Sánchez-Lavega, A., R. Hueso, S. Pérez-Hoyos and J.F. Rojas 2006. A strong vortex in Saturn's south pole. *Icarus* **184**, 524 – 531.

Sánchez-Lavega, A., R. Hueso and S. Pérez-Hoyos, 2006. On the variability of Saturn's Equatorial Jet at cloud top level. *Lecture Notes and Essays on Astrophysics* **II**, 127-138.

Sánchez-Lavega, A., R. Hueso and S. Pérez-Hoyos 2007. The three-dimensional structure of Saturn's equatorial at cloud level. *Icarus* **187**, 510 – 519.

Yanamandra-Fisher, P.A., G. S. Orton, B. M. Fisher, and Sánchez-Lavega. 2001. Saturn's 5.2-μm Cold Spots: Unexpected cloud variability. *Icarus*, **150**, 189 – 193.

Figure captions

Figure 1.

Saturn's southern hemisphere zonal wind profiles up to 80ºS measured by cross-correlation on albedo scans for the CB2 (solid) and MT2 (grey/red) Cassini images. (b) Zonal wind difference between the CB2 and MT2 filters. In both panels a systematic difference of ~20ms^{-1} on the prograde jets, between the two filters, can be seen. (c) Reflectivity scan at MT2 (grey) and CB2 along a meridian 20º away the sub-observer meridian. CB2 reflectivity values are divided by 10. Grey vertical bands mark the jet positions peaks. (d) Individual cloud features tracked in MT2 and CB2 images. Horizontal arrow on the right shows the position of the –42ºS jet peak. Circles highlight features visible only in one of the filters around the jet peak. When tracked they move at different speeds matching the correlation profile in each filter. Squares mark the position of distinct features in the MT2 or CB2 images that move with the same speed outside the eastward jets. The vertical arrow marks the position of an anticyclonic vortex observable in both filters.

Figure 2

Example of one model fitting at 35ºS. Left panel shows the best fitting models (grey lines) compared to the observed reflectivity (solid lines). CB2 reflectivity values are scaled by a factor 1/10. The free model parameter space is shown in the right panel with the corresponding χ^2 contours for each filter that result in cloud height determination.

Altitudes sensed in MT2 and CB2 in the eastward jets

Jet latitude (centric)	P_{MT2} (mbar)	P_{CB2} (mbar)	ΔH
27.5º S	100±40	360±80	1.3±0.7 H
42.0º S	70±10	340±60	1.6±0.3 H
55.5º S	100±20	390±50	1.4±0.4 H
70.5º S	130±70	300±150	1.0±1.0 H

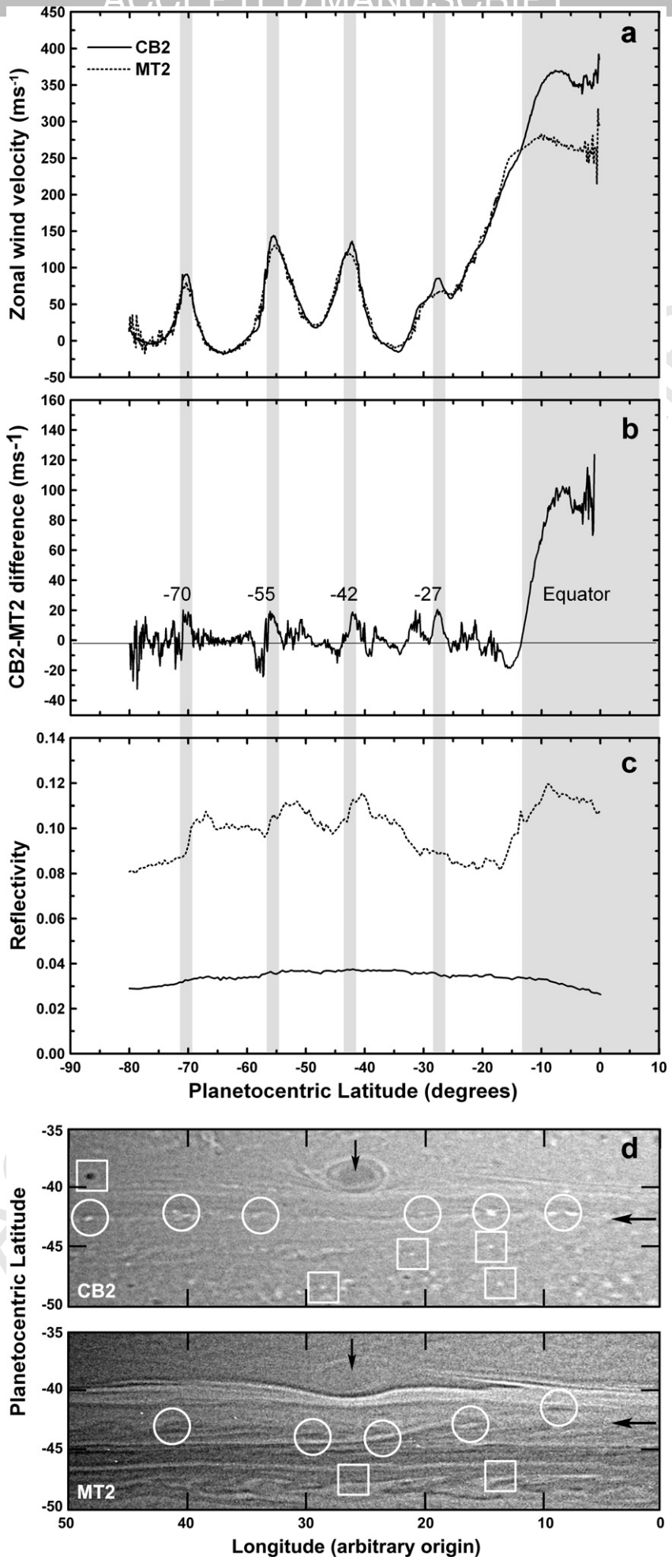

Figure1BW

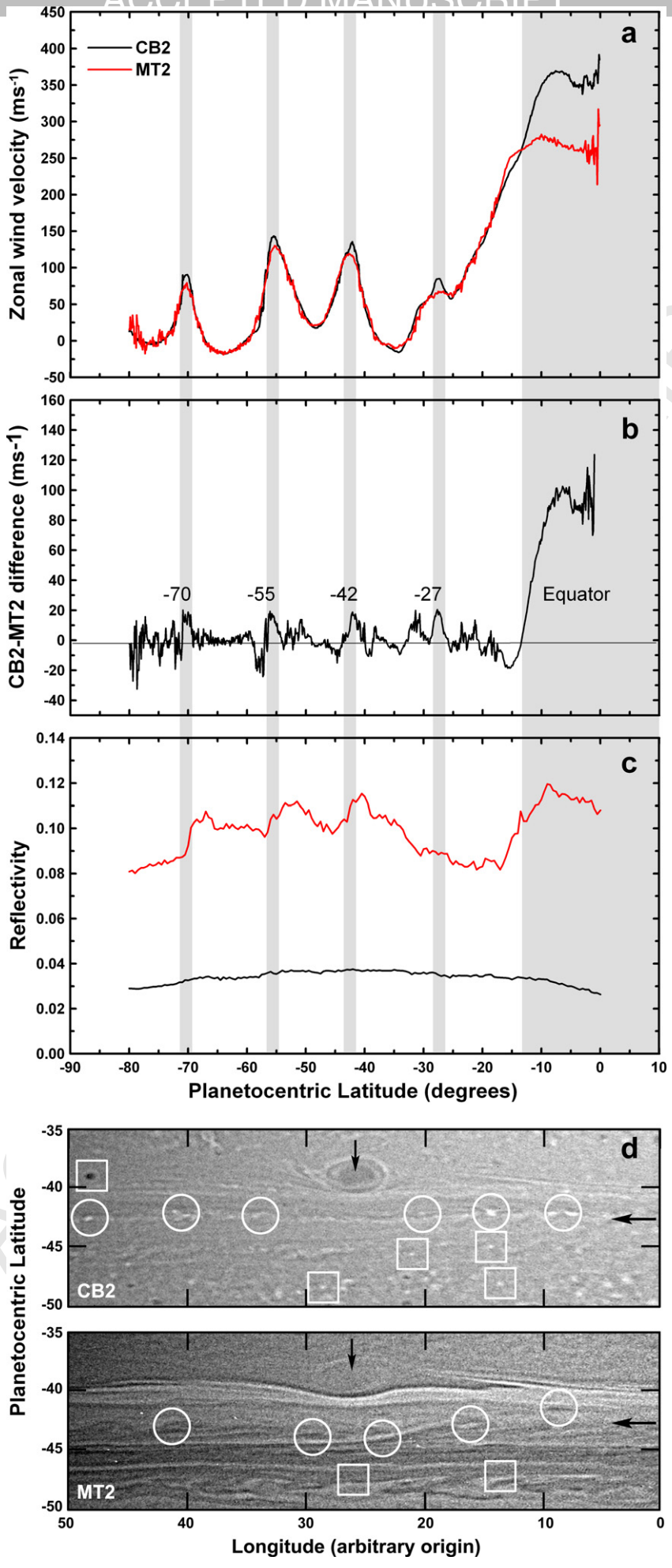

Figure1C

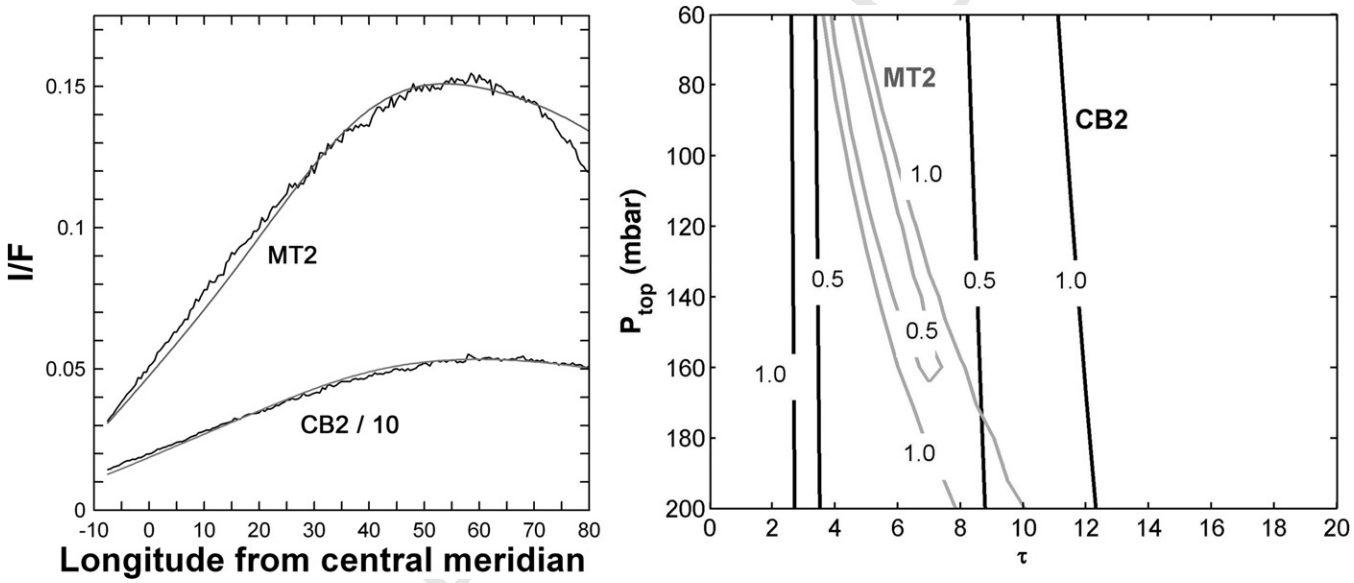

Figure2